Published in final edited form as:
Clin Cancer Res. 2018 August 01; 24(15): 3656–3667. doi:10.1158/1078-0432.CCR-17-3457.

Enhanced Therapeutic Activity of Non-Internalizing Small Molecule-Drug Conjugates Targeting Carbonic Anhydrase IX in Combination With Targeted Interleukin-2

Samuele Cazzamalli[#a], **Barbara Ziffels**[#a], **Fontaine Widmayer**[a], **Patrizia Murer**[a], **Giovanni Pellegrini**[b], **Francesca Pretto**[c], **Sarah Wulhfard**[c], and **Dario Neri**[a,*]

[a]Department of Applied Biosciences, Swiss Federal Institute of Technology (ETH Zürich), Vladimir-Prelog-Weg 4, CH-8093 Zurich (Switzerland) [b]Laboratory for Animal Model Pathology, Institute of Veterinary Pathology, University of Zurich, Winterthurerstrasse 268, CH-8057 Zurich (Switzerland) [c]Philochem AG, Libernstrasse 3, CH-8112 Otelfingen (Switzerland)

[#] These authors contributed equally to this work.

Abstract

Purpose—Antibody-drug conjugates and small molecule-drug conjugates have been proposed as alternatives to conventional anti-cancer cytotoxic agents, with the potential to deliver bioactive payloads to the site of disease, helping spare normal tissues.

Experimental design—Here we describe a novel small molecule-drug conjugate, based on a high-affinity ligand specific to carbonic anhydrase IX. The product featured a peptidic linker, suitable for cleavage in the tumor extracellular environment, and monomethyl auristatin E as cytotoxic payload.

Results—A potent anti-cancer activity was observed in nude mice bearing SKRC-52 renal cell carcinoma xenografts, but no durable complete responses could be observed in this model. However, when the product was administered together with L19-IL2 (a clinical-stage fusion protein capable of delivering interleukin-2 to the tumor neo-vasculature), all treated mice in the combination group could be rendered tumor-free, in a process which favored the influx of natural killer cells into the tumor mass. The combination of L19-IL2 and the new small molecule-drug conjugate also eradicated cancer in 100% of immunocompetent mice, bearing subcutaneously-grafted CT26 colorectal cancer cells, which stably expressed carbonic anhydrase IX.

Conclusion—These findings may be of clinical significance, since carbonic anhydrase IX is over-expressed in the majority of clear-cell renal cell carcinomas and in approximately 30% of colorectal cancers. The targeted delivery of interleukin-2 helps potentiate the action of targeted cytotoxics leading to cancer eradication in models that cannot be cured by conventional chemotherapy.

[*]Corresponding Author: Tel: +41-44-6337401, neri@pharma.ethz.ch.

Disclosure of Potential Conflict of Interest:
D.N. is a co-founder and shareholder of Philogen (www.philogen.com), a Swiss-Italian Biotech company that operates in the field of ligand-based pharmacodelivery

Europe PMC Funders Author Manuscripts

Keywords

Tumor Targeting; Small Molecule Drug Conjugates; Immunocytokines; Carbonic Anhydrase IX; Therapy Studies

Introduction

Cytotoxic drugs are frequently used for cancer chemotherapy [1], but the unfavorable tissue distribution properties of these molecules often prevent dose escalation to therapeutically active regimens [2]. A suboptimal uptake of anti-cancer drugs in the neoplastic masses has been confirmed in cancer patients, using isotope-labeled preparations of drugs and positron emission tomography methodologies [3]. This pharmacokinetic limitation of conventional chemotherapy makes it more difficult to induce objective responses in patients and contributes to side effects [4].

In order to overcome the limitations of conventional cytotoxic agents, it is attractive to couple potent drugs to monoclonal antibodies [5,6] or to small organic ligands [2,7,8], which recognize a cognate antigen in the tumor environment and may therefore facilitate a preferential uptake at the site of disease. While it has long been thought that internalization of drug conjugates into the tumor cell may represent an indispensable requirement for potent anti-cancer activity [9], experimental evidence suggests that it may be possible to release cytotoxic payloads in the tumor extra-cellular space [10–15]. Three Antibody-Drug Conjugates (ADCs) have gained marketing authorization (Kadcyla™, Adcetris™, Besponsa™ and Mylotarg™) for cancer therapy [16], while Small Molecule-Drug Conjugates (SMDCs) are still being investigated both at the preclinical and clinical level [2,7]. SMDCs could offer certain advantages compared to ADCs, such as a more rapid and uniform diffusion into the tumor mass [17], lower cost-of-goods [18] and lack of immunogenicity [19].

Certain folate analogues [20], prostate-specific membrane antigen binders [21], somatostatin antagonists [22] and carbonic anhydrase IX ligands [11,23,24] have been considered as delivery vehicles for SMDC development activities, based on promising tumor-targeting performance in Nuclear Medicine studies [25,26] and on encouraging preclinical results.

Carbonic anhydrase IX (CAIX) is a homodimeric membrane protein that is virtually undetectable in most normal adult tissues, exception made for certain gastrointestinal structures [27]. However, CAIX is up-regulated in hypoxic cells and is over-expressed in approximately 90% of clear-cell renal cell carcinomas, as a result of von Hippel-Lindau inactivation [28]. Interestingly, CAIX is also strongly expressed in a portion of patients with other malignancies, including colorectal, urothelial, lung, stomach, pancreas, breast, head and neck, ovaries, brain and cervix cancer [29]. Antibodies specific to CAIX efficiently localize to metastatic renal cell carcinoma lesions but not to normal gastrointestinal structures, as revealed by immuno-PET studies in cancer patients [30]. Acetazolamide (an approved drug for the treatment of idiopathic intracranial hypertension, metabolic alkalosis and glaucoma) exhibits a high binding affinity to CAIX [31]. The development of charged derivatives of acetazolamide prevents the crossing of the cellular membrane and the binding

to abundant intracellular carbonic anhydrase isoforms [11]. Quantitative biodistribution studies performed in nude mice, bearing SKRC-52 human kidney cancer xenografts, revealed that ^{99m}Tc-labeled charged derivatives of acetazolamide would achieve tumor to blood ratios of ~100:1, six hours after intravenous administration [24,32].

Our group has previously described the synthesis and potent anti-tumor activity of non-internalizing anti-CAIX SMDCs, based on acetazolamide conjugates to DM1, monomethyl auristatin E (MMAE) or the ultrapotent nemorubicin derivative PNU-159682, featuring the use of cleavable disulfide bridges or dipeptide linkers [11,33]. However, we have recently identified the 4,4-bis(4-hydroxyphenyl)valeric acid moiety as a structural feature, capable of increasing the binding affinity of acetazolamide derivatives to CAIX. This allowed the generation of a novel acetazolamide derivative with a higher affinity for CAIX (hereafter named AAZ$^+$) [23], which displays an improved tumor targeting performance, compared to acetazolamide [24,34]. Encour-aged by favorable biodistribution results, we here describe the synthesis and anti-cancer activity of a novel SMDC, based on the high-affinity AAZ$^+$ CAIX-ligand, a cleavable peptide linker and monomethyl auristatin E as cytotoxic payload. We observed that the new SMDC was well tolerated and potently active in preclinical models of cancer that are typically resistant to therapeutic agents which are commonly given to cancer patients. Durable complete cancer eradications could be observed in all treated mice when the new SMDC product was combined with L19-IL2, a clinical-stage fusion protein that delivers interleukin-2 to the alternatively-spliced EDB domain of fibronectin, typically expressed in the sub-endothelial extracellular matrix of tumor blood vessels [35–39]. Collectively, our results provide a rationale for the clinical development of acetazolamide-drug conjugates for the treatment of patients with CAIX-positive malignancies, as well as for their combination with immunostimulatory drugs, such as L19-IL2.

Materials and Methods

Detailed synthetic procedures and characterization of the presented compounds are described in the Supplementary Information.

Peptide synthesis

Peptidic precursors of compounds **1**, **2**, **3** [Figure 1], **5** and **6**, as well as compounds **4**, **7** and **8** were synthesized by solid phase peptide synthesis (SPPS), using Fmoc-protected amino acids. Suitable resins (300-500 mg) were swollen with DMF (10 ml) for 15 min inside a syringe equipped with a filter pad. Fmoc deprotection was achieved by shaking the resin with 20% v/v piperidine in DMF (3 × 5 ml × 10 min). The appropriate Fmoc-protected amino acid (3 eq) was activated with HATU (3 eq) and DIPEA (6 eq) in DMF (5 ml) for 15 min at 0°C. After this time the solution was allowed to react with the resin for 1 hour. Couplings and deprotections were alternated with DMF washing steps (4 × 10 ml), until the desired peptide sequence was obtained on solid phase.

Alkynes bearing acetazolamide or a free amide were then reacted by CuAAC “click” reaction with the corresponding peptide derivatives (carrying an azide moiety) on the resin.

Side chain deprotection, cleavage from the resin, treatment with TCEP (30 eq) and RP-HPLC purification allowed to yield pure peptides, as confirmed by LC/MS analysis.

Conjugates preparation

Commercially available MC-ValCit-PAB-MMAE (1 eq) was reacted with the corresponding precursor (4 eq) in degassed phosphate buffered saline (PBS; 50 mM phosphate, 100 mM NaCl, pH 7.4) added with DMF to help solubility. The reactions were stirred at room temperature until completion (monitored by LC/MS). The solvents were removed under vacuum and the final products were purified through RP-HPLC and lyophilized. The purity (> 95%) of the final compounds was assessed by LC/MS.

Cell cultures

The human renal cell carcinoma cell line SKRC-52 was kindly provided by Professor E. Oosterwijk (Radbound University Nijmegen Medical Centre, Nijmegen, The Netherlands). Upon thawing, cells were kept in culture for no longer than 10 passages. SKRC-52 were maintained in RPMI medium (Invitrogen) supplemented with fetal calf serum (10%, FCS, Invitrogen) and Antibiotic-Antimycotic (1%, AA, Invitrogen) at 37°C and 5% CO_2. For passaging, cells were detached using Trypsin-EDTA 0.05% (Invitrogen) when reaching 90% confluence and re-seeded at a dilution of 1:6.

The murine colorectal carcinoma cell line CT26.wt (ATCC) was maintained in RPMI medium (Invitrogen) supplemented with fetal calf serum (10%, FCS, Invitrogen) and Antibiotic-Antimycotic (1%, AA, Invitrogen) and cultured at 37°C and 5% CO_2. For passaging, confluent cells were detached using Trypsin-EDTA 0.05% (Invitrogen) and re-seeded at a dilution of 1:5. Transfected CT26 cells were kept in the same culture conditions as CT26.wt cells.

Surface plasmon resonance

Surface plasmon resonance (SPR) experiments were performed on a BIAcore™ S200 instrument (GE Healthcare) at room temperature. For all measurements, CM5 chips (Series S) and filtered PBS pH 7.4 with DMSO (5 % v/v) as flow buffer were used. Human CAIX was immobilized on the chip to 500 response units (RU) using EDC·HCl and NHS following manufacturer instructions. Serial dilutions of compounds **1** and **2** [Supplementary Figure 3] in running buffer at a flow rate of 20 μL min^{-1} were used as analytes. After each cycle, the sensor surface was regenerated by a short treatment with DMSO (50 % v/v) in PBS. Sensorgrams were solvent corrected and the binding kinetics were analyzed with the BIAcore™ S200 evaluation software using a 1:1 Langmuir.

In vitro cytotoxicity assay

SKRC-52 cells were seeded in 96-well plates in RPMI added with 10% FCS (100 μl) at a density of 5×10^3 cells per well and allowed to grow for 24 hours. The medium was replaced with medium containing different concentrations of test substance (1:3 dilution steps) and plates were incubated under standard culture conditions. After 72 hours the medium was removed, MTS cell viability dye (20 μl, Promega) was added in 150 μl of fresh medium, the plates were incubated for 2 hours under standard culture conditions and the

absorbance at 490 nm was measured on a Spectra Max Paradigm multimode plate reader (Molecular Devices; background correction was performed by measuring the absorbance at 630 nm). Experiments were performed in triplicates and the average cell viability was calculated as measured background corrected absorbance divided by the absorbance of untreated control wells. IC50 values were determined by fitting data to the four-parameter logistic equation, using a Prism 6 software (GraphPad Software) for data analysis.

FACS analysis

For cellular expression analysis of human CAIX, cells were detached with 50 mM EDTA and 5×10^5 cells were stained with a human anti-CAIX specific antibody (500 nM, 1 hour, 4°C) in a volume of 100 µl FACS-Buffer (0.5% BSA, 2 mM EDTA in PBS). For signal amplification, the anti-CAIX antibody was detected with an anti-human AlexaFluor647 labeled antibody (Invitrogen) (1:200, 45 min, 4°C). In-between and after staining, cells were washed with 100 µl FACS-Buffer and centrifuged at 1100 rpm for 3 min. Stained cells were analyzed with a 2L-Cytoflex (Beckman-Coulter). SKRC-52 cells were used as positive control and CT26.wt cells as negative control. Results were analyzed with FlowJo 9 (FlowJo LLC).

QIFIKIT® (Agilent) was used to quantify the copy number of human CAIX on SKRC-52 and CT26.3E10 cells. The cells were detached with 50 mM EDTA and 10^6 cells were stained with a human anti-CAIX specific antibody (500 nM, 1 hour, 4°C) in a volume of 100 µl FACS-Buffer (0.5% BSA, 2 mM EDTA in PBS). For signal amplification, the anti-CAIX antibody was detected with an anti-human AlexaFluor488 labeled antibody (Invitrogen) (1:200, 45 min, 4°C). In-between and after staining, cells were washed twice with 3 mL of FACS-Buffer and centrifuged at 1100 rpm for 5 min. Set-up and calibration beads present in the commercial kit were stained with an Alexa488 antibody (Invitrogen) (1:200, 45 min, 4°C). Cells and beads were analyzed with a LSR Fortessa (Becton Dickinson & Co.). Results were analyzed with FlowJo 9 (FlowJo LLC). Calibration curve was obtained plotting the fluorescent intensity with the number of antigen of the different bead populations, and CAIX expression determined based on the fluorescent intensity of stained SKRC-52 and CT26.3E10 cells [Supplementary Figure 11].

Transfection of human CAIX in CT26 tumor cells and monoclonal selection

The gene for human CAIX was cloned into the mammalian expression vector pcDNA3.1(+) [Figure 5A] containing an antibiotic resistance for G418 Geneticin. 6×10^7 CT26.wt cells were transfected with 60 µg of pcDNA3.1(+) containing the human CAIX gene using the Amaxa™ 4D-Nucleofector (Lonza) with the SG Cell Line 4D-Nucleofector® X Kit L (Lonza) and reseeded in complete growing medium. Three days after the transfection, the medium was replaced with RPMI (10% FCS, 1% AA) containing 0.5 mg/ml G418 (Merck) to select a stably transfected polyclonal cell line. To yield a monoclonal cell line, the stable cell line was stained as described for FACS analysis and single cell sorting was performed using a BD FACSAria III. Different clones were expanded and checked for antigen expression. Clone CT26.3E10 was selected for CAIX expression by FACS, immunofluorescence and confocal microscopic, and used for further *in vivo* experiments.

Europe PMC Funders Author Manuscripts

Animal studies

All animal experiments were conducted in accordance with Swiss animal welfare laws and regulations under the license number 27/2015 granted by the Veterinäramt des Kantons Zürich.

Implantation of subcutaneous tumors

SKRC-52 cells were grown to 80% confluence and detached with Trypsin-EDTA 0.05% (Life Technologies). Cells were washed with Hank's Balanced Salt Solution (HBSS, pH 7.4) once, counted and re-suspended in HBSS to a final concentration of 3.4×10^7 cells ml^{-1}. Aliquots of 5×10^6 cells (150 µl of the suspension) were injected subcutaneously in the right flank of female athymic BALB/c nu/nu mice (8-10 weeks of age, Janvier).

CT26.3E10 cells were grown to 80% confluence and detached with Trypsin-EDTA 0.05% (Life Technologies). Cells were washed with Hank's Balanced Salt Solution (HBSS, pH 7.4) once, counted and re-suspended in HBSS to a final concentration of 6.0×10^7 cells ml^{-1}. Aliquots of 6×10^6 cells (100 µl of the suspension) were injected subcutaneously in the right flank of female BALB/c mice (8-10 weeks of age, Janvier).

IVIS imaging

Female BALB/c mice bearing subcutaneous CT26.3E10 or CT26.wt tumors were injected intravenously with acetazolamide labeled with the near infrared dye moiety IRDye680RD (AAZ-IRDye680RD; compound **6**; 250 nmol/Kg), dissolved in sterile PBS (100 µl). Mice were anesthetized with isoflurane and fluorescence images acquired on an IVIS Spectrum imaging system (Xenogen, exposure 1s, binning factor 8, excitation at 675 nm, emission filter at 720 nm, f number 2, field of view 13.1). Images were taken before the injection and after 5 min, 1 hour, 3 hours and 6 hours. Food and water were given ad libitum during that period. Mice were sacrificed after the last picture by cervical dislocation and organs were extracted and imaged using the indicated parameters.

Radiolabelling and quantitative biodistribution studies

Radiolabeling procedures with technetium-99m were performed following described procedures [24]. Briefly, compounds **7**, **8** and **9** (60 nmol) in TBS pH 7.4 (50 µl) were separately mixed with $SnCl_2$ (Sigma Aldrich, 200 µg) and sodium glucoheptonate (TCI, 20 mg) in H_2O (150 µl). Trisbuffered saline at pH 7.4 (600 µl) was added and the resulting solution degassed for 5 min by bubbling with nitrogen gas. The eluate from a ^{99m}Tc-generator (200 µl, ca. 200 MBq, Mallinckrodt) was added and the reaction mixture heated to 90 °C for 20 min. After cooling to room temperature, analytic aliquots were analyzed by RP-HPLC (XTerra C18, 5% MeCN in 0.1% aq. TFA to 80% over 20 min on a Merck-Hitachi D-7000 HPLC system equipped with a Raytest Gabi Star radiodetector) to determine radiolabelling yields. Technetium-99m incorporations >95% were routinely achieved.

SKRC-52 tumor cells were implanted into female BALB/c nu/nu mice (Janvier) as described above, and allowed to grow for three weeks to an average volume of 250 mm^3. Mice were randomized (n = 3 per group) and injected intravenously with radiolabelled preparations of **compounds 7**, **8** and **9** (1-3 MBq, 30 nmol/Kg). Mice were sacrificed 6 hours after the

injection by CO_2 asphyxiation and organs extracted, weighted and radioactivity measured with a Packard Cobra γ-counter. Values are expressed as %ID/g ± SD [Supplementary Figure 1].

The tumor targeting performance of L19-IL2 in SKRC-52 bearing nude mice was evaluated by quantitative biostribution analysis of the radioiodinated protein as described previously [40]. Briefly, radioiodinated protein was injected into the lateral tail vein of mice (n = 3). The animals were sacrificed after 24 hours, organs were excised and radioactivity was counted in Cobra gamma counter (Packard). Values are expressed as %ID/g ± SD [Supplementary Figure 5].

Therapy experiments

SKRC-52 or CT26.3E10 tumor cells were implanted into female BALB/c mice (Janvier) as described above, and allowed to grow to an average volume of 100 mm^3. Mice were randomly assigned into therapy groups of 4 or 5 animals and treatment started by injecting a solution of AAZ-ValCit-MMAE (compound **1**), AAZ^+-ValCit-MMAE (compound **2**), untargeted control (compound **3**), L19-IL2, combination or vehicle (PBS containing 1% of DMSO) intravenously (lateral tail vein) at the doses and with the schedules indicated in the text and in Figures 2, 3 and 6. Compounds **1**, **2** and **3** were injected as solutions in sterile PBS containing 1% DMSO. L19-IL2 was injected as solution in appropriate sterile formulation buffer (Philogen). Animals were weighed and tumor sizes measured daily with an electronic caliper. The tumor volume was calculated according to the formula (long side) × (short side) × (short side) × 0.5. Animals were sacrificed when the termination criteria were reached. Prism 6 software (GraphPad Software) was used for data analysis (regular two-way ANOVA followed by Bonferroni test).

Histology, immunofluorescence and immunohistochemistry studies

SKRC-52 tumors were excised, snap-frozen in OCT medium (Thermo Scientific) and stored at - 80°C. Cryostat sections (7 μm) were cut, fixed with acetone and stained with hematoxylin and eosin (H&E) using routine methods or subjected to immunofluorescence and immunohistochemistry. Primary staining for NK cells was performed with a rat anti-murine NKp46 IgG (NCR1; Biolegend). Primary staining for apoptosis was performed with a rabbit anti-caspase 3 IgG (C8487; Sigma Aldrich). Donkey anti-rat IgG-AlexaFluor594 and goat anti-rabbit IgG-AlexaFluor488 (Molecular Probes by Life Technologies) were then used for microscopic detection as secondary antibodies. Inflammatory cell infiltration of the tumors was assessed by immunostaining with a rat anti-CD45 monoclonal antibody (ab25386, Abcam, Cambridge, UK; 1:2000). The reaction was visualized using 3,3'-diaminobenzidine (DAB) as chromogen, followed by light counterstain with hematoxylin). Double immunohistochemistry was applied to frozen tumor sections to detect neutrophils (anti-myeloperoxidase rabbit polyclonal antibody, A0398, Dako-Agilent Technologies, Denmark; 1:1000) and macrophages (anti-CD68 rabbit polyclonal antibody, ab125212, Abcam,; 1:200). The reaction was visualized using 3-amino-9-ethylcarbazole (AEC) and DAB as chromogens for neutrophils and macrophages respectively, followed by hematoxylin counterstain.

Images were obtained using an Axioskop2 mot plus microscope (Zeiss) or the NDP.view2 software (Hamamatsu Photonics K.K., Japan), after the slides were scanned using a digital slide scanner (NanoZoomer-XR C12000, Hamamatsu Photonics K.K.).

For further evaluation of human CAIX expression 10^5 cells were cultured overnight on a sterile covers slip. Cells were fixed with ice-cold acetone, blocked with PBS (2% BSA) and stained with 5 μg/ml of a human antibody anti-CAIX in PBS (1% BSA). Detection was performed with an anti-human AlexaFluor488-labeled antibody (1:200 in PBS containing 1% BSA). The cytoskeleton was stained with Phalloidin-AlexaFluor647 (ThermoFisher) and cell nuclei were stained with DAPI (MolecularProbes). Microscopic analysis was performed with an Axioskop 2 mot plus microscope (Zeiss) [Supplementary Figure 10].

To determine CAIX internalization after transfection, CT26.3E10 cells were seeded into 4-well cover slip chamber plates (Sarstedt) at a density of 10^4 cells per well in RPMI medium (1 mL, Invitrogen) supplemented with 10% FCS, 1% AA and 10 mM HEPES and allowed to grow for 24 hours under standard culture conditions. The medium was replaced with medium containing AAZ-Alexa594 (compound **5**; 120 nM) [Supplementary Information], after 1 hour Hoechst 33342 nuclear dye (Invitrogen) was added and randomly selected colonies imaged on a SP8 confocal microscope equipped with an AOBS device (Leica Microsystems).

Results

In vivo biodistribution of AAZ^+ and AAZ derivatives

The tumor-targeting performance of AAZ^+, an affinity-matured version of acetazolamide discovered using encoded self-assembling chemical libraries and previously characterized by nearinfrared fluorescence imaging [23], was confirmed in mice with subcutaneously-grafted SKRC-52 tumors, using a radiolabeled and fluorescently labeled AAZ^+ derivative [Supplementary Figure 1 and Supplementary Figure 2]. The product accumulated with 40% ID/g in the tumor mass six hours after intravenous administration (with a tumor to blood ratio of 80:1), while a similar compound featuring acetazolamide (AAZ) as CAIX binder exhibited a 18% ID/g at the same time point. Encouraged by these favorable biodistribution results, we synthesized a novel SMDC product, featuring the AAZ^+ structure as tumor-homing moiety.

Synthesis and *in vitro* activity of acetazolamide SMDC derivatives

SMDC products were designed following the general ligand-spacer-linker-drug scheme depicted in Figure 1. The CAIX-ligand acetazolamide was installed by copper-catalyzed azide-alkyne cycloaddition (“Click” reaction) on solid phase onto different peptides, which featured the presence or the absence of a 4,4-bis(4-hydroxyphenyl)valeric acid moiety, responsible for high-affinity CAIX binding [23]. The resulting SMDCs **1** and **2** were subsequently cleaved and purified. In addition, compound **3** (which served as negative control) was synthesized in a similar way, replacing the acetazolamide moiety with an amide and thus generating a structure devoid of CAIX binding [Figure 1]. Reduction of a C-terminal cysteine residue allowed the coupling to a linker-payload, featuring a Val-Cit

cleavable linker, a self-immolating para-aminobenzyl carbamate and the potent anti-tubulin monomethyl auristatin E (MMAE), which is also used in Adcetris™. All products were obtained as highly pure (> 95% purity by UPLC) lyophilized material [Supplementary Information], characterized for the binding to the cognate antigen [Supplementary Figure 3] and used for the subsequent biological assays.

The cytotoxic activity of compound AAZ^+-ValCit-MMAE **2** was tested on SKRC-52 cells and compared to the anti-proliferative properties of free MMAE, used as reference compound [Supplementary Figure 4]. As expected for acetazolamide derivatives of MMAE, compound **2** acted as a pro-drug and exhibited a substantially higher IC_{50} value (440 nM) compared to MMAE (IC_{50} = 0.9 nM). This experimental observation is in line with what had previously been published for several non-internalizing SMDC derivatives bearing the same linker-payload structure [33].

Therapy experiments in SKRC-52 renal cell carcinoma model

We compared the anticancer activity of compounds AAZ-ValCit-MMAE (**1**) and AAZ^+-ValCit-MMAE (**2**) in BALB/c nude mice, bearing subcutaneously-grafted SKRC-52 renal cell carcinomas. Compound **3**, devoid of the CAIX-targeting moiety but otherwise identical to compound **2**, served as negative control. The SMDCs were administered at the maximum tolerated dose, which had been found to be 250 nmol/Kg in preliminary experiments [Supplementary Figure 5], following the schedule depicted in Figure 2. A fourth group of mice (“presaturation” group) was injected with a 50-fold higher dose (12.5 μmol/Kg) of ligand AAZ^+, which was directly followed by the administration of AAZ^+-ValCit-MMAE (**2**). Both compounds **1** and **2** showed a potent anti-cancer activity ($p<0.0001$ compared to the group of mice treated with vehicle), while negative control compound **3** did not display a difference from the vehicle-treated group. Presaturation with AAZ^+ partially reduced therapeutic activity. Compound **2** was very well tolerated [Figure 2B] and exhibited the most potent tumor growth retardation effect, but none of the mice enjoyed a durable complete response.

In a second therapy experiment performed in the same cancer model, compound **2** (AAZ^+-ValCit-MMAE) was tested in combination with the clinical-stage antibody-cytokine fusion protein L19-IL2 [36–39] [Figure 3]. A selective uptake of L19-IL2 at the tumor site had been confirmed in the SKRC-52 model, using biodistribution studies and a radioiodinated protein preparation [Supplementary Figure 6]. While neither L19-IL2 nor compound **2** were able to eradicate SKRC-52 xenografts when used as single agent, the combination of the two agents was well tolerated and induced complete remissions in all mice [Figure 3 and Supplementary Figure 7]. Cured mice were re-challenged 17 days after the therapy by a second subcutaneous injection of cancer cells and tumors regrew in all cases, as expected considering the lack of functional T cells in nude mice. Macroscopically, the combination of SMDC with L19-IL2 induced flattening of the tumor and hematoma formation at the site previously occupied by the solid tumor. Histologically, xenografts from mice that had received the vehicle or the monotherapy were composed of coalescing sheets and nests of densely packed neoplastic epithelial cells, separated by inconspicuous fibrous stroma and mild infiltration of inflammatory cells [Figure 4 and Supplementary Figure 8]. Tumors from

mice exposed to the combination therapy exhibited instead a marked increase in the number of CD45-positive inflammatory cells infiltrating the xenograft. Most inflammatory cells were p46-positive NK cells [Figure 4 and Supplementary Figure 9]. Moreover, combination treatment led to a potent and homogenous induction of apoptosis within the tumor mass, as revealed by cleaved caspase 3 staining [Figure 4]. Infiltration by myeloperoxidase-positive neutrophils and CD68-positive macrophages was low in all groups and restricted to the periphery of the xenografts [Figure 4].

Therapy experiments in immunocompetent mice, bearing syngeneic CT26.3E10 tumors

Approximately 30% of patients with colorectal cancer express high levels of CAIX in their tumor, but the immunocompetent mouse models of the disease tested by our group were negative for the antigen (see for example FACS analysis on CT26.wt murine cancer cells included in Figure 5B; similar results were obtained for C51.wt and for RENCA tumor cells). In order to establish an immunocompetent murine model of colorectal cancer expressing CAIX, we stably-transfected colorectal CT26.wt cancer cells with a gene coding for human CAIX and a second gene conferring antibiotic resistance against Neomycin [Figure 5A]. After antibiotic selection and single cell sorting, monoclonal cell lines were tested for CAIX expression. Clone CT26.3E10 (but not CT26.wt) showed a shift in fluorescence intensity in FACS analysis using an anti-CAIX monoclonal antibody. The FACS shift was similar to the one observed for SKRC-52 cells [Figure 5B]. Fluorescence microscopy experiments confirmed CAIX expression on the membrane of CT26.3E10 and SKRC-52 cells, but not in wild type CT26 cells [Figure 5C and Supplementary Figure 10]. CAIX quantification by FACS analysis indicates that CT26.3E10 has a slightly lower surface density of CAIX, compared to SKRC-52 cells [Supplementary Figure 11]. Furthermore, mice bearing CT26.3E10 tumors showed a preferential uptake of the near-infrared fluorophore conjugate AAZ-IRdye680RD in the neoplastic mass 6 hours after intravenous injection, compared to similar experiments performed in mice bearing CT26.wt tumors [Figure 5D].

Therapy experiments were then performed using compound **2**, alone or in combination with the immunocytokine L19-IL2, in immunocompetent BALB/c mice bearing subcutaneous CT26.3E10 tumors. Also in this case, the antitumor effect was strongest when both therapeutic agents were used in combination ($p<0.0001$), leading to durable complete responses in 100% of treated mice [Figure 6 and Supplementary Figure 12]. 37 days after complete tumor eradication, cured mice were re-challenged by a second subcutaneous injection of CT26.3E10 cancer cells and tumors regrew in all cases. The observation that the combination treatment was not able to confer protective immunity to the treated animals is in keeping with the predominant role played by NK cells, following L19-IL2 accumulation in the neoplastic mass [35].

Discussion

An acetazolamide derivative (named AAZ^{+}), which recognizes CAIX with dissociation constant in the subnanomolar range, was coupled to the linker-payload combination of Adcetris™ (an approved ADC product), featuring the valine-citrulline dipeptide, a self-

immolative linker and the anti-tubulin agent MMAE. The new SMDC product mediated a potent tumor growth inhibition activity, but was not able to induce durable complete remissions, when used as single agent in tumor-bearing mice. However, the same product, used in combination with L19-IL2, mediated complete cancer eradication in all nude mice with xenografted SKRC-52 renal cell carcinomas, as well as in all immunocompetent mice bearing a syngeneic CT26 colorectal cancer, transfected with human CAIX.

L19-IL2 is a fully human antibody-cytokine fusion protein [35], which has been extensively studied in preclinical models of cancer and in clinical trials in patients with various types of malignancies [36,39]. Encouraged by the results observed in Phase II studies [37,38], the product is currently being investigated in a Phase III clinical trial as combination agent for the treatment of resectable Stage IIIB,C melanoma (NCT02938299), which is authorized in the U.S.A., Germany, Italy and Poland.

From a mechanistic viewpoint, the antibody-based delivery of interleukin-2 to the tumor environment promotes the influx of leukocytes into the neoplastic mass [35,41,42] and an increase in vascular permeability at the tumor site [41,43], favoring a preferential uptake of other therapeutic agents used in combination. The observation that L19-IL2 displays a similar activity in nude mice and in immunocompetent mice bearing the same murine tumor suggests that, at least in mice, the product mediates an anti-cancer effect by inducing the migration, proliferation and activation of NK cells [35,42]. The use of tumor-targeting antibody fusions as an avenue to increase the therapeutic index of interleukin-2 has been described also in reports published by other groups [44,45].

The targeted delivery of interleukin-2 to the sub-endothelial extracellular matrix in solid tumors and in certain hematological malignancies has been shown to synergize with other therapeutic modalities, such as the use of chemotherapy [41], radiotherapy [46], intact antibodies capable of triggering an Antibody-Dependent Cell Cytotoxicity (ADCC) [42], as well as various forms of armed antibody derivatives. A synergistic therapeutic activity has been reported for the combination of IL2-based immunocytokines with other antibody-cytokine fusion proteins (e.g., those based on TNF or on interleukin-12) [47,48] and for ADC products [49].

CAIX has initially been assumed to be an internalizing antigen, suitable for the intracellular delivery and release of potent cytotoxic payloads coupled to CAIX-specific antibodies [50]. However, subsequent studies have clearly shown that CAIX does not efficiently internalize, at least when bound to small molecule ligands [11]. The targeted delivery of linker-payload combinations to the extracellular environment is attractive, as it may promote an efficient drug release process, triggered by high local concentration of glutathione (released by dying tumor cells) [11,12] or by proteases [10,33]. Potent cytotoxic drugs may diffuse into the tumor mass, thus potentially acting also on neighboring tumor cells, endothelial cells and/or tumor-resident leukocytes.

The combined use of L19-IL2 with the SMDC product **2** (AAZ^{+}-ValCit-MMAE) leads to cancer eradication in two mouse models, which do not respond to conventional chemotherapy or to other experimental therapeutic strategies [11]. Since the corresponding

targets (i.e., the alternativelyspliced EDB domain of fibronectin and CAIX) are strongly expressed in the majority of patients with clear-cell renal cell carcinoma and in various types of other malignancies (including colorectal cancer), the preclinical results presented in this study provide a rationale for the clinical investigation of this combination modality. A companion diagnostic, featuring the use of acetazolamide derivatives labeled with technetium-99m, has exhibited promising results in biodistribution studies and has recently received authorization to start clinical studies, with SPECT imaging of cancer patients (EUDRACT n° 2016-004909-13). The study will be important, in order to elucidate whether similar tumor:organ and tumor:blood ratios can be observed both in mice and in patients. Ideally, the SMDC + L19-IL2 combination should be administered to those subjects, who show an adequate uptake of acetazolamide derivatives in the neoplastic masses, using Nuclear Medicine procedures [25].

Supplementary Material

Refer to Web version on PubMed Central for supplementary material.

Acknowledgements

We thank Dr. Nikolaus Krall for his contribution to the biodistribution experiments of Supplementary Figure 1. We acknowledge the positive and constructive criticisms made by Dr. Alberto Dal Corso. The authors gratefully acknowledge financial support from ETH Zürich, the Swiss National Science Foundation (Projects Nr. 310030B_163479/1, SINERGIA CRSII2_160699/1), ERC Advanced Grant “Zauberkugel” (Grant Agreement 670603) and Kommission für Technologie und Innovation (Grant Nr. 17072.1).

Financial Support:

The authors gratefully acknowledge financial support from ETH Zürich, the Swiss National Science Foundation (Projects Nr. 310030B_163479/1, SINERGIA CRSII2_160699/1), ERC Advanced Grant “Zauberkugel” (Grant Agreement 670603) and Kommission für Technologie und Innovation (Grant Nr. 17072.1)

References

[1]. Pratt WB, Ruddon RW, Ensminger WD, Maybaum J. The Anticancer Drugs. Oxford University Press; New York, Oxford: 1994.

[2]. Krall N, Scheuermann J, Neri D. Small targeted cytotoxics: current state and promises from DNA-encoded chemical libraries. Angew Chem Int Ed Engl. 2013; 52(5):1384–402. [PubMed: 23296451]

[3]. van der Veldt AA, Lubberink M, Mathijssen RH, Loos WJ, Herder GJ, Greuter HN, et al. Toward prediction of efficacy of chemotherapy: a proof of concept study in lung cancer patients using [(1)(1)C]docetaxel and positron emission tomography. Clin Cancer Res. 2013; 19(15):4163–73. [PubMed: 23620410]

[4]. Van Cutsem E, Moiseyenko VM, Tjulandin S, Majlis A, Constenla M, Boni C, et al. Phase III study of docetaxel and cisplatin plus fluorouracil compared with cisplatin and fluorouracil as first-line therapy for advanced gastric cancer: a report of the V325 Study Group. J Clin Oncol. 2006; 24(31):4991–7. [PubMed: 17075117]

[5]. Doronina SO, Toki BE, Torgov MY, Mendelsohn BA, Cerveny CG, Chace DF, et al. Development of potent monoclonal antibody auristatin conjugates for cancer therapy. Nat Biotechnol. 2003; 21(7):778–84. [PubMed: 12778055]

[6]. Chari RV, Miller ML, Widdison WC. Antibody-drug conjugates: an emerging concept in cancer therapy. Angew Chem Int Ed Engl. 2014; 53(15):3796–827. [PubMed: 24677743]

[7]. Srinivasarao M, Galliford CV, Low PS. Principles in the design of ligand-targeted cancer therapeutics and imaging agents. Nat Rev Drug Discov. 2015; 14(3):203–19. [PubMed: 25698644]

[8]. Herzog TJ, Kutarska E, Bidzinsk M, Symanowski J, Nguyen B, Rangwala RA, et al. Adverse Event Profile by Folate Receptor Status for Vintafolide and Pegylated Liposomal Doxorubicin in Combination, Versus Pegylated Liposomal Doxorubicin Alone, in Platinum-Resistant Ovarian Cancer: Exploratory Analysis of the Phase II PRECEDENT Trial. Int J Gynecol Cancer. 2016; 26(9):1580–85. [PubMed: 27654255]

[9]. Sievers EL, Senter PD. Antibody-drug conjugates in cancer therapy. Annu Rev Med. 2013; 64:15–29. [PubMed: 23043493]

[10]. Dal Corso A, Cazzamalli S, Gebleux R, Mattarella M, Neri D. Protease-Cleavable Linkers Modulate the Anticancer Activity of Noninternalizing Antibody-Drug Conjugates. Bioconjug Chem. 2017; 28(7):1826–33. [PubMed: 28662334]

[11]. Krall N, Pretto F, Decurtins W, Bernardes GJ, Supuran CT, Neri D. A small-molecule drug conjugate for the treatment of carbonic anhydrase IX expressing tumors. Angew Chem Int Ed Engl. 2014; 53(16):4231–5. [PubMed: 24623670]

[12]. Perrino E, Steiner M, Krall N, Bernardes GJ, Pretto F, Casi G, et al. Curative properties of noninternalizing antibody-drug conjugates based on maytansinoids. Cancer Res. 2014; 74(9): 2569–78. [PubMed: 24520075]

[13]. Bernardes GJ, Casi G, Trussel S, Hartmann I, Schwager K, Scheuermann J, et al. A traceless vascular-targeting antibody-drug conjugate for cancer therapy. Angew Chem Int Ed Engl. 2012; 51(4):941–4. [PubMed: 22173886]

[14]. Du X, Beers R, Fitzgerald DJ, Pastan I. Differential cellular internalization of anti-CD19 and -CD22 immunotoxins results in different cytotoxic activity. Cancer Res. 2008; 68(15):6300–5. [PubMed: 18676854]

[15]. Caculitan NG, Dela Cruz Chuh J, Ma Y, Zhang D, Kozak KR, Liu Y, et al. Cathepsin B Is Dispensable for Cellular Processing of Cathepsin B-Cleavable Antibody-Drug Conjugates. Cancer Res. 2017; 77(24):7027–37. [PubMed: 29046337]

[16]. Lambert JM, Berkenblit A. Antibody-Drug Conjugates for Cancer Treatment. Annu Rev Med. 2018; 69:191–207. [PubMed: 29414262]

[17]. Yuan F, Dellian M, Fukumura D, Leunig M, Berk DA, Torchilin VP, et al. Vascular permeability in a human tumor xenograft: molecular size dependence and cutoff size. Cancer Res. 1995; 55(17):3752–6. [PubMed: 7641188]

[18]. Firer MA, Gellerman G. Targeted drug delivery for cancer therapy: the other side of antibodies. J Hematol Oncol. 2012; 5:70. [PubMed: 23140144]

[19]. Kuriakose A, Chirmule N, Nair P. Immunogenicity of Biotherapeutics: Causes and Association with Posttranslational Modifications. J Immunol Res. 2016; 2016 1298473.

[20]. Leamon CP, Parker MA, Vlahov IR, Xu LC, Reddy JA, Vetzel M, et al. Synthesis and biological evaluation of EC20: a new folate-derived, (99m)Tc-based radiopharmaceutical. Bioconjug Chem. 2002; 13(6):1200–10. [PubMed: 12440854]

[21]. Hillier SM, Maresca KP, Lu G, Merkin RD, Marquis JC, Zimmerman CN, et al. 99mTc-labeled small-molecule inhibitors of prostate-specific membrane antigen for molecular imaging of prostate cancer. J Nucl Med. 2013; 54(8):1369–76. [PubMed: 23733925]

[22]. Ginj M, Zhang H, Waser B, Cescato R, Wild D, Wang X, et al. Radiolabeled somatostatin receptor antagonists are preferable to agonists for in vivo peptide receptor targeting of tumors. Proc Natl Acad Sci U S A. 2006; 103(44):16436–41. [PubMed: 17056720]

[23]. Wichert M, Krall N, Decurtins W, Franzini RM, Pretto F, Schneider P, et al. Dual-display of small molecules enables the discovery of ligand pairs and facilitates affinity maturation. Nat Chem. 2015; 7(3):241–9. [PubMed: 25698334]

[24]. Krall N, Pretto F, Mattarella M, Muller C, Neri D. A technetium 99m-labeled ligand of carbonic anhydrase IX selectively targets renal cell carcinoma in vivo. J Nucl Med. 2016

[25]. Morris RT, Joyrich RN, Naumann RW, Shah NP, Maurer AH, Strauss HW, et al. Phase II study of treatment of advanced ovarian cancer with folate-receptor-targeted therapeutic (vintafolide) and

companion SPECT-based imaging agent (99mTc-etarfolatide). Ann Oncol. 2014; 25(4):852–8. [PubMed: 24667717]

[26]. Rahbar K, Ahmadzadehfar H, Kratochwil C, Haberkorn U, Schafers M, Essler M, et al. German Multicenter Study Investigating 177Lu-PSMA-617 Radioligand Therapy in Advanced Prostate Cancer Patients. J Nucl Med. 2017; 58(1):85–90. [PubMed: 27765862]

[27]. Hilvo M, Rafajova M, Pastorekova S, Pastorek J, Parkkila S. Expression of carbonic anhydrase IX in mouse tissues. J Histochem Cytochem. 2004; 52(10):1313–22. [PubMed: 15385577]

[28]. Wichert M, Krall N. Targeting carbonic anhydrase IX with small organic ligands. Curr Opin Chem Biol. 2015; 26:48–54. [PubMed: 25721398]

[29]. Lv PC, Roy J, Putt KS, Low PS. Evaluation of Nonpeptidic Ligand Conjugates for the Treatment of Hypoxic and Carbonic Anhydrase IX-Expressing Cancers. Mol Cancer Ther. 2017; 16(3):453–60. [PubMed: 27980101]

[30]. Oosterwijk E, Bander NH, Divgi CR, Welt S, Wakka JC, Finn RD, et al. Antibody localization in human renal cell carcinoma: a phase I study of monoclonal antibody G250. J Clin Oncol. 1993; 11(4):738–50. [PubMed: 8478666]

[31]. Supuran CT. Acetazolamide for the treatment of idiopathic intracranial hypertension. Expert Rev Neurother. 2015; 15(8):851–6. [PubMed: 26154918]

[32]. Cazzamalli S, Dal Corso A, Neri D. Acetazolamide serves as selective delivery vehicle for dipeptide-linked drugs to renal cell carcinoma. Mol Cancer Ther. 2016

[33]. Cazzamalli S, Corso AD, Neri D. Linker stability influences the anti-tumor activity of acetazolamide-drug conjugates for the therapy of renal cell carcinoma. J Control Release. 2017; 246:39–45. [PubMed: 27890855]

[34]. Yang X, Minn I, Rowe SP, Banerjee SR, Gorin MA, Brummet M, et al. Imaging of carbonic anhydrase IX with an 111In-labeled dual-motif inhibitor. Oncotarget. 2015; 6(32):33733–42. [PubMed: 26418876]

[35]. Carnemolla B, Borsi L, Balza E, Castellani P, Meazza R, Berndt A, et al. Enhancement of the antitumor properties of interleukin-2 by its targeted delivery to the tumor blood vessel extracellular matrix. Blood. 2002; 99(5):1659–65. [PubMed: 11861281]

[36]. Eigentler TK, Weide B, de Braud F, Spitaleri G, Romanini A, Pflugfelder A, et al. A dose-escalation and signal-generating study of the immunocytokine L19-IL2 in combination with dacarbazine for the therapy of patients with metastatic melanoma. Clin Cancer Res. 2011; 17(24):7732–42. [PubMed: 22028492]

[37]. Weide B, Eigentler TK, Pflugfelder A, Zelba H, Martens A, Pawelec G, et al. Intralesional treatment of stage III metastatic melanoma patients with L19-IL2 results in sustained clinical and systemic immunologic responses. Cancer Immunol Res. 2014; 2(7):668–78. [PubMed: 24906352]

[38]. Danielli R, Patuzzo R, Di Giacomo AM, Gallino G, Maurichi A, Di Florio A, et al. Intralesional administration of L19-IL2/L19-TNF in stage III or stage IVM1a melanoma patients: results of a phase II study. Cancer Immunol Immunother. 2015; 64(8):999–1009. [PubMed: 25971540]

[39]. Johannsen M, Spitaleri G, Curigliano G, Roigas J, Weikert S, Kempkensteffen C, et al. The tumour-targeting human L19-IL2 immunocytokine: preclinical safety studies, phase I clinical trial in patients with solid tumours and expansion into patients with advanced renal cell carcinoma. Eur J Cancer. 2010; 46(16):2926–35. [PubMed: 20797845]

[40]. Borsi L, Balza E, Bestagno M, Castellani P, Carnemolla B, Biro A, et al. Selective targeting of tumoral vasculature: comparison of different formats of an antibody (L19) to the EDB domain of fibronectin. Int J Cancer. 2002; 102(1):75–85. [PubMed: 12353237]

[41]. Moschetta M, Pretto F, Berndt A, Galler K, Richter P, Bassi A, et al. Paclitaxel enhances therapeutic efficacy of the F8-IL2 immunocytokine to EDA-fibronectin-positive metastatic human melanoma xenografts. Cancer Res. 2012; 72(7):1814–24. [PubMed: 22392081]

[42]. Schliemann C, Palumbo A, Zuberbuhler K, Villa A, Kaspar M, Trachsel E, et al. Complete eradication of human B-cell lymphoma xenografts using rituximab in combination with the immunocytokine L19-IL2. Blood. 2009; 113(10):2275–83. [PubMed: 19005180]

[43]. Hornick JL, Khawli LA, Hu P, Sharifi J, Khanna C, Epstein AL. Pretreatment with a monoclonal antibody/interleukin-2 fusion protein directed against DNA enhances the delivery of therapeutic molecules to solid tumors. Clin Cancer Res. 1999; 5(1):51–60. [PubMed: 9918202]

[44]. Gubbels JA, Gadbaw B, Buhtoiarov IN, Horibata S, Kapur AK, Patel D, et al. Ab-IL2 fusion proteins mediate NK cell immune synapse formation by polarizing CD25 to the target cell-effector cell interface. Cancer Immunol Immunother. 2011; 60(12):1789–800. [PubMed: 21792658]

[45]. Klein C, Waldhauer I, Nicolini VG, Freimoser-Grundschober A, Nayak T, Vugts DJ, et al. Cergutuzumab amunaleukin (CEA-IL2v), a CEA-targeted IL-2 variant-based immunocytokine for combination cancer immunotherapy: Overcoming limitations of aldesleukin and conventional IL-2-based immunocytokines. Oncoimmunology. 2017; 6(3):e1277306. [PubMed: 28405498]

[46]. Rekers NH, Zegers CM, Yaromina A, Lieuwes NG, Biemans R, Senden-Gijsbers BL, et al. Combination of radiotherapy with the immunocytokine L19-IL2: Additive effect in a NK cell dependent tumour model. Radiother Oncol. 2015; 116(3):438–42. [PubMed: 26138057]

[47]. Schwager K, Hemmerle T, Aebischer D, Neri D. The immunocytokine L19-IL2 eradicates cancer when used in combination with CTLA-4 blockade or with L19-TNF. J Invest Dermatol. 2013; 133(3):751–8. [PubMed: 23096716]

[48]. Pasche N, Wulhfard S, Pretto F, Carugati E, Neri D. The antibody-based delivery of interleukin-12 to the tumor neovasculature eradicates murine models of cancer in combination with paclitaxel. Clin Cancer Res. 2012; 18(15):4092–103. [PubMed: 22693354]

[49]. Gutbrodt KL, Casi G, Neri D. Antibody-based delivery of IL2 and cytotoxics eradicates tumors in immunocompetent mice. Mol Cancer Ther. 2014; 13(7):1772–6. [PubMed: 24759429]

[50]. Petrul HM, Schatz CA, Kopitz CC, Adnane L, McCabe TJ, Trail P, et al. Therapeutic mechanism and efficacy of the antibody-drug conjugate BAY 79-4620 targeting human carbonic anhydrase 9. Mol Cancer Ther. 2012; 11(2):340–9. [PubMed: 22147747]

Europe PMC Funders Author Manuscripts

Europe PMC Funders Author Manuscripts

Statement of Translational Relevance

The antibody-based delivery of interleukin-2 to the tumor environment can be used to potentiate the therapeutic activity of targeted cytotoxic agents. In this article, we have combined the clinical-stage fusion protein L19-IL2 with a small molecule-drug conjugate, capable of selective homing to tumor cells, expressing carbonic anhydrase IX on their surface. In two mouse models of cancer, durable complete responses could be observed in 100% of mice which had received the combination treatment, while the antibody-cytokine fusion and the small-molecule drug conjugate could only provide tumor growth retardation. Studies of leukocyte infiltration into the tumor mass evidence an important role played by natural killer cells, a prominent target of interleukin-2 activity. These findings may be of clinical relevance, since renal cell carcinomas and certain other malignancies exhibit a strong carbonic anhydrase IX expression

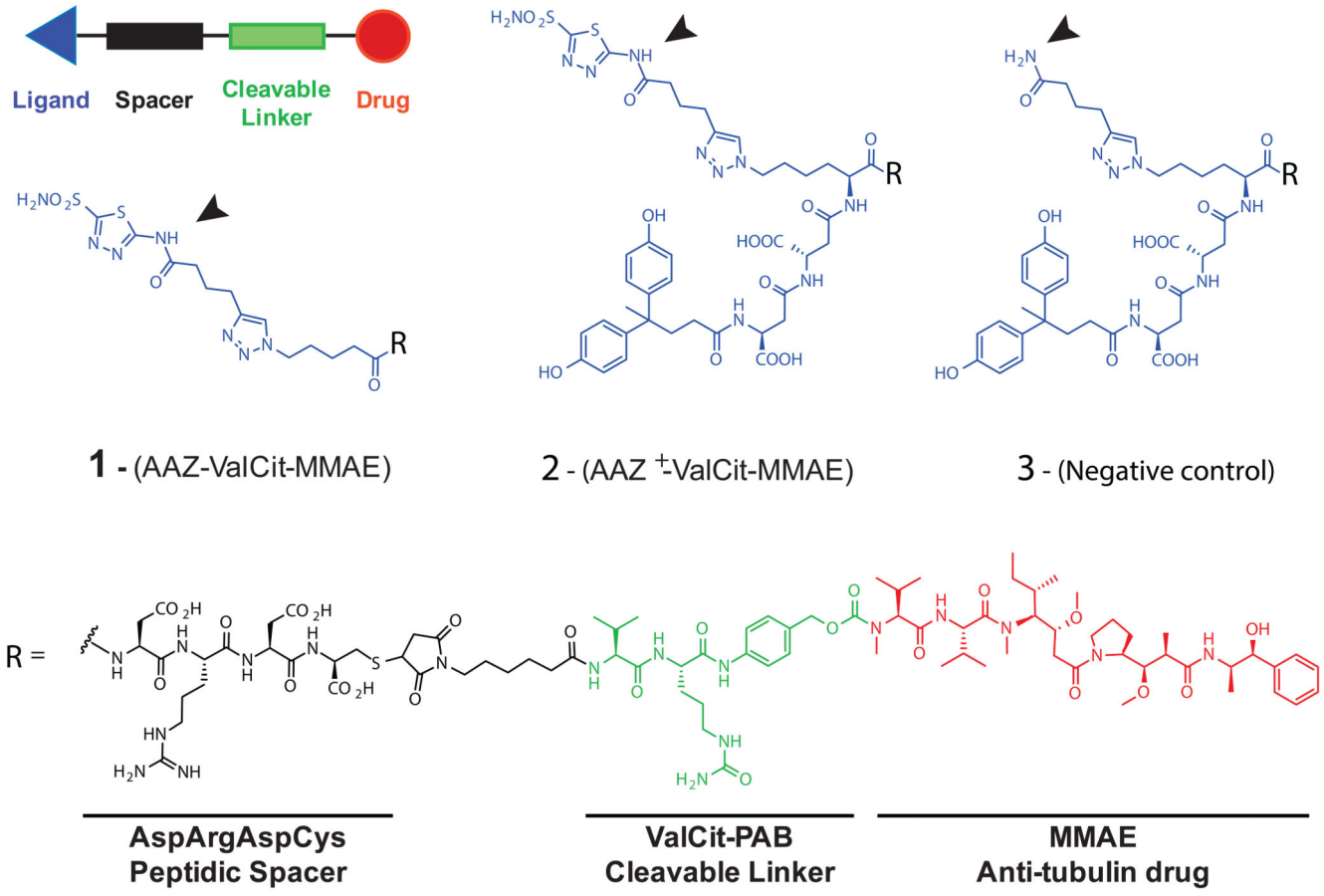

Figure 1. General scheme of Small Molecule-Drug Conjugates (SMDCs) and chemical structures of CAIX-targeting SMDCs.

Compounds display an acetazolamide targeting ligand (AAZ; compound **1**), an affinity matured version of acetazolamide (AAZ^{+}; compound **2**) or an amide (serving as negative control; compound **3**). All products feature the cytotoxic payload MMAE, an Asp-Arg-Asp-Cys peptide spacer, a Valine-Citrulline (ValCit) dipeptide cleavable linker and a *p*-amino benzyl (PAB) self-immolative linker.

Europe PMC Funders Author Manuscripts

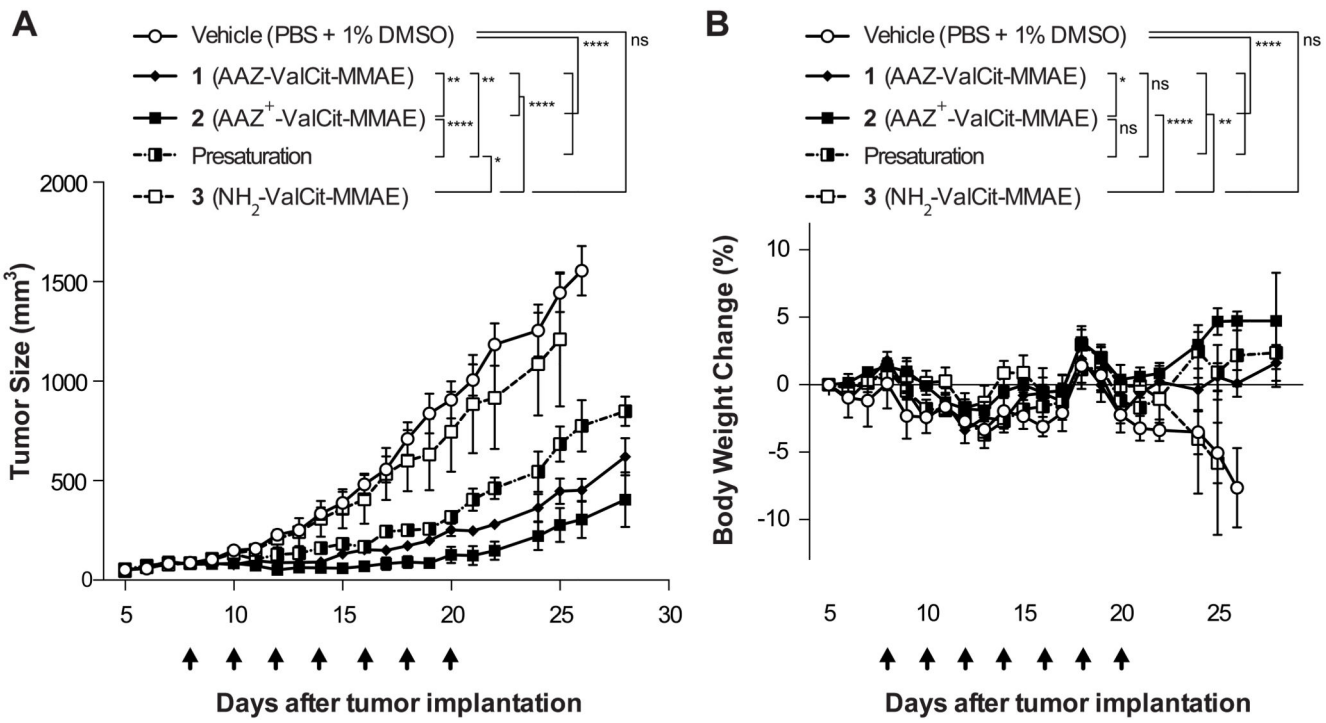

Figure 2. Comparison of the *In vivo* efficacy of AAZ-ValCit-MMAE and AAZ$^+$-ValCit-MMAE (compounds 1 and 2) in BALB/c nu/nu mice bearing subcutaneous SKRC-52 renal cell carcinomas.

Cytotoxic derivative **3** devoid of the acetazolamide moiety was used as negative control. All the compounds were injected intravenously at the dose of 250 nmol/Kg per administration. The "presaturation" group was treated with a 50-fold dose of AAZ$^+$ ligand (1.25 μmol/Kg; compound **4**) directly followed by an administration of compound **2** (250 nmol/Kg). Graph (A) compares the therapeutic activity of the different treatment. Data points represent mean tumor volume ± SEM, n = 4 per group. SMDC **2** based on the affinity matured AAZ$^+$ ligand exhibited a superior antitumor activity when compared with SMDC **1**, based on the non-matured AAZ targeting moiety. The therapeutic efficacy of SMDC **2** was reduced significantly by the presaturation with an excess of free AAZ$^+$. In graph (B) percentage changes of body weight during the experiment are represented. **** indicates $p<0.0001$; ** indicates $p<0.01$; * indicates $p<0.05$; ns indicates $p>0.05$ (2-way ANOVA test, followed by Bonferroni post-test).

Europe PMC Funders Author Manuscripts

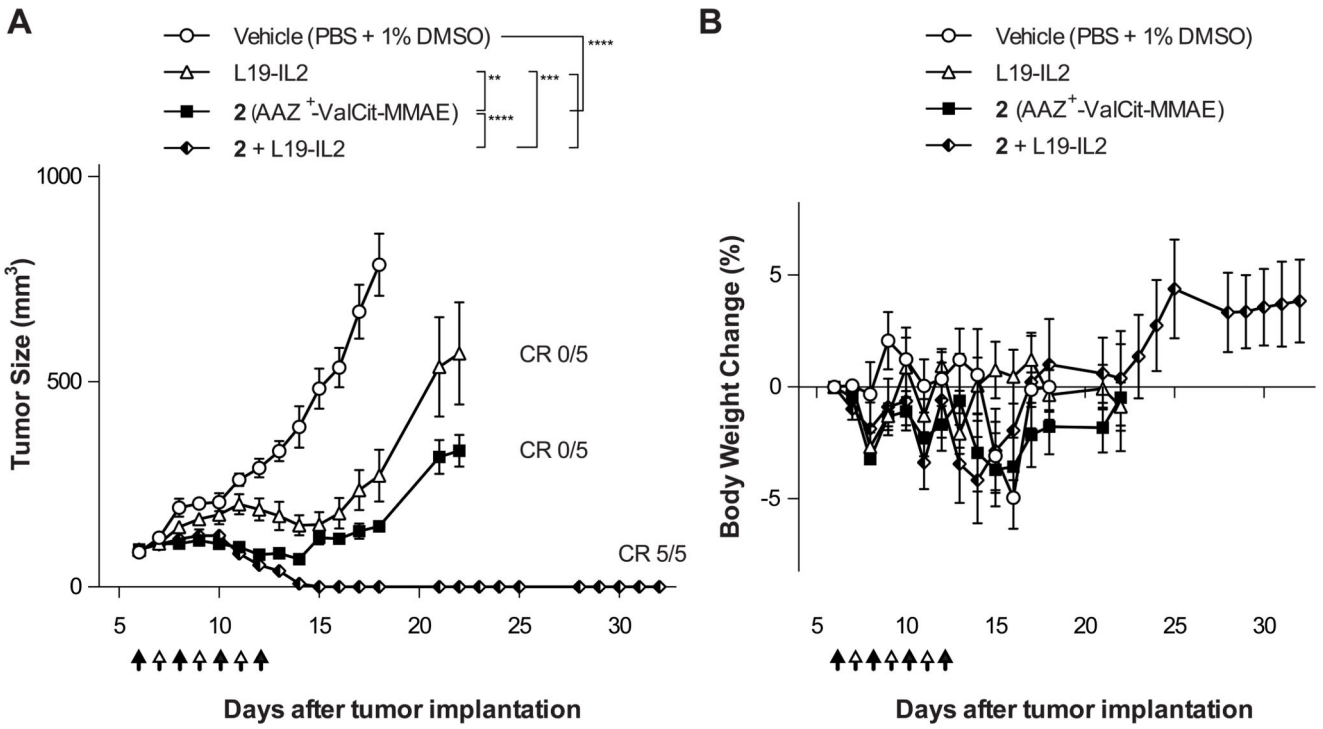

Figure 3. Therapeutic activity of AAZ^{+}-ValCit-MMAE in combination with the immuno-cytokine L19-IL2 in BALB/c nu/nu mice bearing SKRC-52 renal cell carcinoma.

Nude mice bearing established subcutaneous tumors were treated with AAZ^{+}-ValCit-MMAE (compound **2**; 250 nmol/kg; IV; black arrow) and L19-IL2 (2.5 mg/Kg; IV; white arrow), as monotherapy or in a combination regimen. Graph (A) compares the therapeutic activity of the different treatment. Data points represent mean tumor volume ± SEM, n = 5 per group. CR = Complete Responses. In graph (B) percentage changes of body weight during the experiment are represented. **** indicates $p<0.0001$; *** indicates $p<0.001$; ** indicates $p<0.01$ (2-way ANOVA test, followed by Bonferroni post-test).

Europe PMC Funders Author Manuscripts

Europe PMC Funders Author Manuscripts

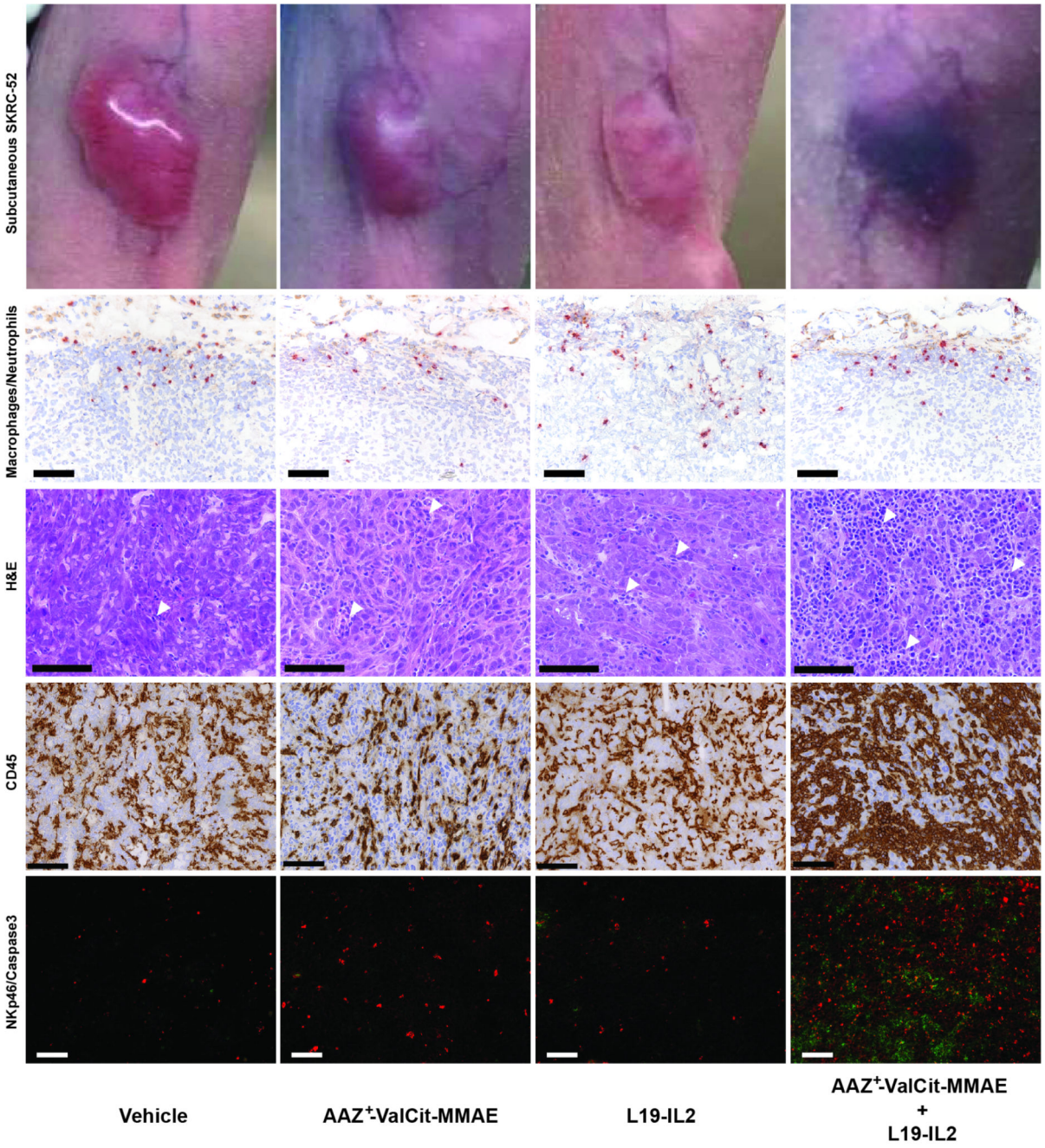

Figure 4. Ex vivo histological and immunofluorescence analysis on SKRC-52 tumor sections following treatment with vehicle, AAZ^{+}-ValCit-MMAE (SMDC), L19-IL2 (immunocytokine) or the AAZ^{+}-ValCit-MMAE/L19-IL2 combination.

Representative images of mice treated with saline, single agents or combination. H&E staining of tumor samples is depicted at a 30X magnification. Immunofluorescence analysis of tumor samples is depicted at a 10X magnification. Green = NKp46 staining; Red = Caspase 3 staining; Blue = DAPI staining. Immunohistochemistry analysis of tumor samples is depicted at a 20X magnification (scale bars: 100 μm). Red = myeloperoxidase-positive neutrophils; Brown = CD68-positive macrophages or CD45. Moderate numbers of

neutrophils and macrophages infiltrate the periphery of all xenografts, without meaningful difference between the different therapy groups. A marked increase in infiltrating inflammatory cells (white arrowheads) is observed following treatment with the AAZ^{+}-ValCit-MMAE/L19-IL2 combination. Increased numbers of infiltrating NK cells, associated with higher numbers of neoplastic apoptotic cells, are detected in the same group. All H&E pictures are taken from the center of the xenografts. The homogenous eosinophilic appearance observed in the nuclei of the neoplastic cells from the vehicle xenograft represents a freezing artifact.

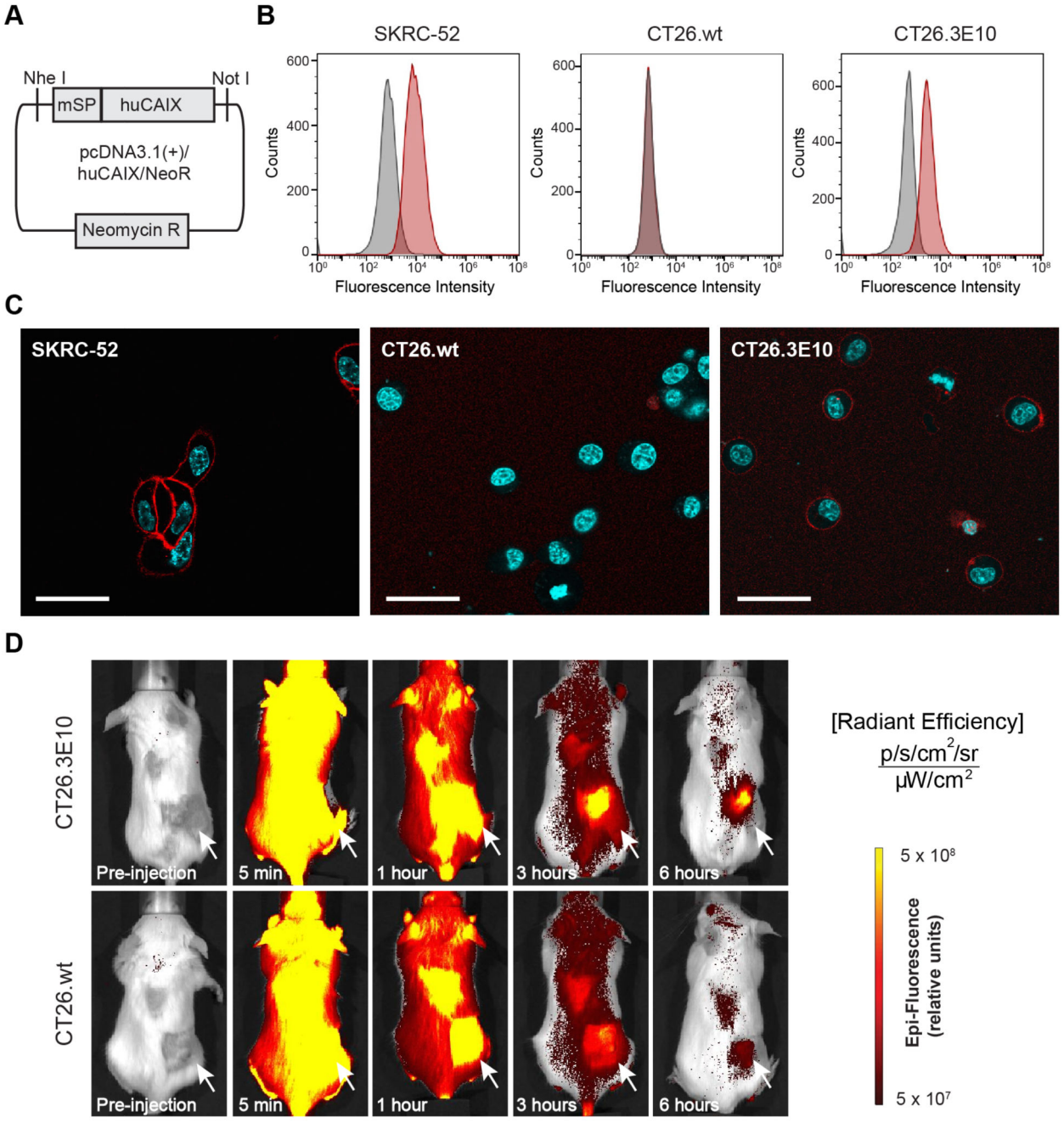

Figure 5. *In vitro* and *in vivo* evaluation of the new murine colorectal carcinoma model CT26.3E10 transfected with the human antigen CAIX.

(A) Cloning scheme of human CAIX in pcDNA3.1(+). (B) FACS analysis for expression of human CAIX on SKRC-52, CT26.wt and transfected CT26.3E10 cells. Staining was performed with a human anti-CAIX specific antibody and the corresponding signal was amplified with an anti-human AlexaFluor488 secondary antibody. (C) Confocal microscopy analysis on living SKRC-52, CT26.wt and CT26.3E10 cells after exposure to acetazolamide labeled with AlexaFluor594 (AAZ-AlexaFluor594; **5**) (120 nM) at 1 hour incubation time.

Europe PMC Funders Author Manuscripts

The conjugate is mainly found at the cell surface in CT26.3E10 and in the positive control SKRC-52. No cell surface binding can be detected for the negative control CT26.wt. Red = AAZ-AlexaFluor594 staining; Blue = Hoechst 33342 staining; Scale bar = 100 μm. (D) Evaluation of the *in vivo* targeting performance of AAZ-IRdye680RD (**4**) in immunocompetent BALB/c mice bearing CAIX transfected CT26.3E10 tumors by near-infrared fluorescence imaging. A selective tumor uptake at early time points (3 and 6 hours) was observed, in comparison to the biodistribution of the molecule in CAIX-negative CT26.wt tumor bearing mice.

Europe PMC Funders Author Manuscripts

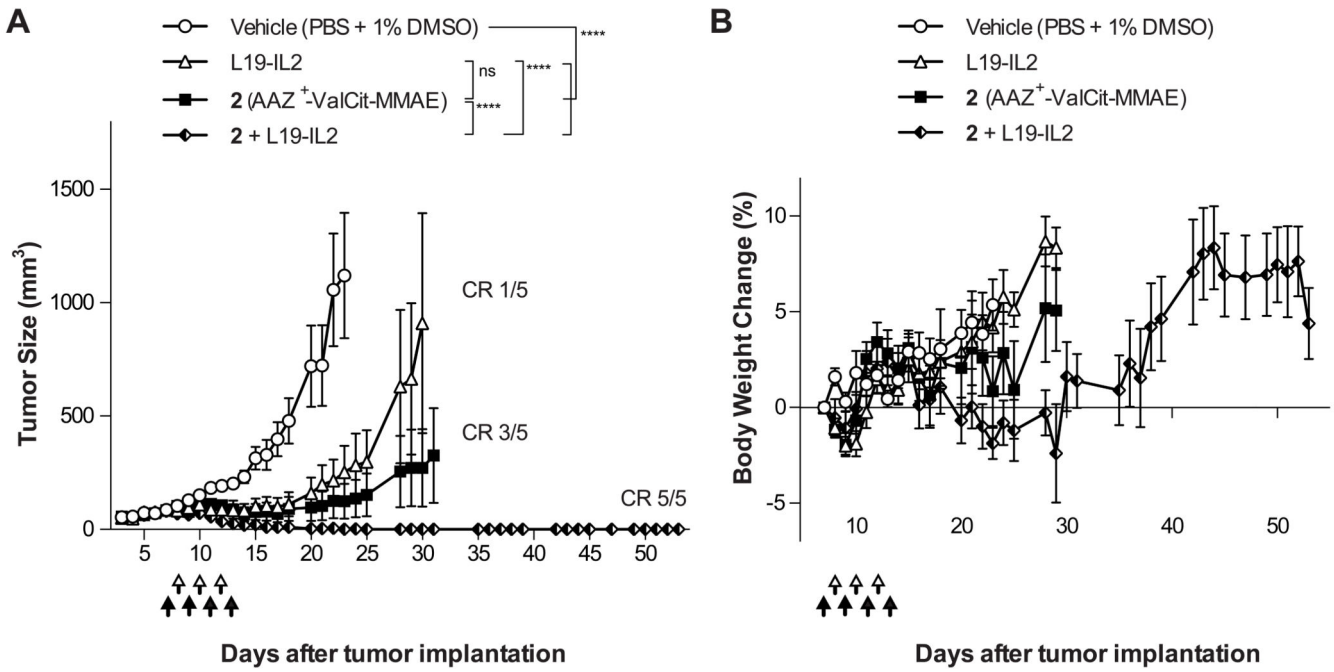

Figure 6. Therapeutic activity of AAZ^{+}-ValCit-MMAE in combination with the immunocytokine L19-IL2 in BALB/c mice bearing CT26.3E10 colorectal carcinoma.

BALB/c mice bearing established subcutaneous, human CAIX expressing tumors were treated with AAZ^{+}-ValCit-MMAE (compound **2**; 250 nmol/kg; IV; black arrow) and L19-IL2 (2.5 mg/Kg; IV; white arrow), as monotherapy or in a combination regimen. Graph (A) compares the therapeutic activity of the different treatments. Data points represent mean tumor volume ± SEM, n = 5 per group. CR = Complete Responses. In graph (B) percentage changes of body weight during the experiment are represented. **** indicates $p<0.0001$; *** indicates $p<0.001$; ** indicates $p<0.01$ (2-way ANOVA test, followed by Bonferroni post-test).

Europe PMC Funders Author Manuscripts